Available online at www.sciencedirect.com
ScienceDirect
Vision Research 47 (2007) 2934–2942
Vision Research
www.elsevier.com/locate/visres

Ocular aberrations in barn owl eyes

Wolf M. Harmening [a,*], Michael A. Vobig [b], Peter Walter [b], Hermann Wagner [a]

[a] Department of Zoology and Animal Physiology, RWTH Aachen University, Kopernikusstrasse 16, 52056 Aachen, Germany
[b] Department of Ophthalmology, RWTH Aachen University, Pauwelsstrasse 30, 52074 Aachen, Germany

Received 8 June 2007; received in revised form 31 July 2007

Abstract

Optical quality in barn owl eyes is presented in terms of measuring the ocular wavefront aberrations with a standard Tscherning-type wavefront aberrometer under natural viewing conditions. While accommodative state was uncontrolled, all eyes were focused within 0.4 D with respect to the plane of the aberrometer. Total RMS wavefront error was between 0.06 and 0.15 μm (mean: 0.10 μm, STD: 0.03 μm, defocus cancelled) for a 6 mm pupil. The results suggest that image quality in barn owl eyes is excellent.

Keywords: Wavefront aberration; Tscherning principle; Modulation transfer function; Point-spread function; Convolution; Animal vision; Barn owl

1. Introduction

The barn owl is an excellent candidate for studies of orientation behaviour both in the auditory and visual domain, because it displays several functional, anatomical and physiological specializations. The most prominent feature of vision in these birds are the frontally oriented eyes, which create a large binocular field of view, an indicator for increased ethological importance of the use of stereo vision (Martin, 1984; Martin & Katzir, 1999; Wagner & Luksch, 1998). Consistently, behavioural studies showed that barn owls possess global stereopsis and use disparity as a depth cue with hyperacute precision (Nieder & Wagner, 2001; van der Willigen, Frost, & Wagner, 1998, 2003). Electrophysiological studies revealed that the visual Wulst of barn owls shows a high degree of binocular interactions and contains disparity sensitive cells that are tuned to characteristic disparities (Pettigrew & Konishi, 1976; Wagner & Frost, 1993, 1994). A more recent study found that barn owls also can discriminate non-aligned features in visual stimuli on a hyperacute level when viewed monocularily (Harmening, Göbbels, & Wagner, 2007), a phenomenon known as vernier acuity in human visual research. This study also pointed to a similar computation of vernier targets in humans and owls, because the results in owls displayed a typical crowding/masking effect and a threshold improvement by a similar ratio which is typical for binocular summation in vernier experiments conducted with human subjects (Banton & Levi, 1991; Harmening et al., 2007; Malania, Herzog, & Westheimer, 2007).

Objective measurements of the metrics of the barn owl eye implicated that these eyes are designed to maximize image quality while maintaining an increased level of retinal information convergence, advantageous especially under low light conditions (Martin, 1982; Schaeffel & Wagner, 1996). With an axial length of about 17.5 mm, the barn owl eye is relatively large (Schaeffel & Wagner, 1996), being almost twice as long as allometry based on body weight would suggest (Howland, Merola, & Basarab, 2004). Generally, a larger eye results in a larger retinal image, and thus, in an improved resolving power. On the other hand, indirect measurements of normal visual acuity (i.e. grating acuity estimation by ganglion cell counts and by pattern electro-retinogram) showed that visual acuity in these birds is comparably poor (Ghim & Hodos, 2006; Wathey & Pettigrew, 1989). Here, we wanted to find out to what degree

* Corresponding author. Fax: +49 241 8022133.
E-mail address: wolf@bio2.rwth-aachen.de (W.M. Harmening).

0042-6989/$ - see front matter © 2007 Elsevier Ltd. All rights reserved.
doi:10.1016/j.visres.2007.08.001

vision in the owl is limited by the optical properties of their eyes. For that purpose we studied optical quality in means of an objective measurement of the ocular wavefront aberrations with a standard Tscherning-type aberrometer in the awake barn owl under natural viewing conditions.

Wavefront aberrometry for the assessment of optical quality in human eyes has been widely used and can also be often found in clinical applications directly linked to eye surgery (Marcos, 2006; Thibos, Applegate, & Marcos, 2003; Thibos, Hong, Bradley, & Cheng, 2002). Besides human eye studies, the measurement of wave aberrations was also applied in animal eye studies. So far, these include wavefront-error reports in eyes of mice (de la Cera, Rodriguez, Llorente, Schaeffel, & Marcos, 2006), cats (Huxlin, Yoon, Nagy, Porter, & Williams, 2004), chicken (Thibos, Cheng, Phillips, & Collins, 2002), tree shrews (Ramamirtham, Norton, Siegwart, & Roorda, 2003) and monkeys (Coletta, Troilo, Moskowitz, Nickla, & Marcos, 2003; Ramamirtham et al., 2006, 2005).

2. Materials and methods

2.1. Subjects

Experimental animals were four adult American barn owls (*Tyto alba pratincola,* three males, one female). Subject ages were between one and three years. All owls were taken from the institute's breeding stock and were hand-raised. They were kept in aviaries throughout their lives. All owls carried a "head-holder", a small aluminium stick, that was implanted onto the skull of their forehead under anaesthesia at an earlier time during life (for details of the procedure see (Nieder & Wagner, 1999)). Animals were kept at about ninety percent of their free feeding weight, because they participated in other behavioural experiments in which food deprivation was essential. A single measurement session was conducted with each owl and lasted no longer than three hours. Care and treatment of the owls were carried out in accordance with the guidelines for animal experimentation as approved by the "Landespräsidium für Natur, Umwelt und Verbraucherschutz Nordrhein Westfalen", Recklinghausen, Germany, and complied with the "NIH Guide for the use and care of laboratory animals".

2.2. Measurement protocol and aberrometer

All measurements were conducted at the Department of Ophthalmology in Aachen. The experimental room was lit dimly by tungsten light, producing a luminance between 2 and 7 cd/m^2 at the walls, the experimental table and the aberrometer, which matched the luminance of the fixation target inside the aberrometer. Barn owls were sitting on a wooden perch that was attached to the experimental table directly in front of the aberrometer (see Fig. 1a). After a short period of adaptation to the lightning conditions the experiment was started. One of the experimenters held the tame owl and its head in a natural viewing position. Since barn owls lack any eye movements, relative eye position could be controlled by adjusting the head position. The correct alignment of the head and, thus, the eye in front of the aberrometer was achieved by constantly monitoring pupil size and shape. After a few attempts the animals were used to this procedure and showed good cooperation. No drugs were given to lubricate the eye, enlarge pupils or block accommodation. The owls blinked normally during the imaging session (i.e. about six times/minute).

The aberrometer was a Tscherning-type system (Schwind Eye Tech Solutions, Kleinostheim, Germany), with a 660 nm laser-diode illumination source and 168 measuring spots. Measuring acuity and reproducibility of this machine was tested with artificial and natural eyes of known error before measurements were conducted, and lay in the normal range (±0.08 D for defocus and cylinder, 0.02 μm for higher order aberrations (Mrochen, Kaemmerer, Mierdel, Krinke, & Seiler, 2000)). A schematic sketch of the aberrometer's general components can be found in Fig. 1b. The pupil was illuminated by six infrared (IR) diodes that were circularly arranged around the aperture of the aberrometer. The corneal image together with a set of superimposed aiding lines was constantly monitored by a CMOS camera and, thus, provided reliable centring and focusing of the pupil. Purkinje reflexes of the IR diodes were always held well within the inner part of the pupil (compare Fig. 1c). The whole system was mounted on a moving stage which was quickly adjustable in all three spatial dimensions to align the aberrometer aperture with the subject's pupil and to adjust focus. A single measurement took less than 50 ms. During this time an array of parallel laser beams of known spatial configuration was projected onto the retina of the measured eye and its retinal reflection was recorded by indirect ophthalmoscopy with a CMOS low-light camera. Typical images consisted of about 140 reflection spots (exemplary retinal image in Fig. 1d). The measuring procedure was repeated in the same way for each eye several times (6–26 repetitions). Image analysis was carried out offline after each measurement session.

2.3. Data analysis

In total, eight eyes of four owls were studied in four measurement sessions. In each session 6–26 retinal images for each eye were recorded. With the application of a centroiding algorithm fitting the intensity profiles of each illumination spot to a Gaussian function in the retinal image, relative spot displacement was recorded. From these displacements the underlying wavefront was calculated and expressed in terms of the Zernike polynomial expansion up to the sixth-order. Individual Zernike coefficients and the orthonormal set of Zernike polynomials, as recommended for describing wave aberration functions (Thibos, Applegate, Schwiegerling, & Webb, 2000), are presented in this study. The orthonormal set of Zernike terms and orders are also called the root-mean-square (RMS) wavefront error contribution of that term or orders. Ordering convention of single Zernike terms followed the OSA standards for reporting the optical aberrations of eyes (Thibos, Applegate, Schwiegerling, & Webb, 2002). The RMS of a single Zernike term was calculated according to:

$$\mathrm{RMS}(Z_n^m) = c_n^m \cdot \sqrt{\frac{2\cdot(n+1)}{1+i}} \quad \text{with } i=0 \text{ if } m\neq 0, \text{and } i=1 \text{ if } m=0 \tag{1}$$

(with c, Zernike coefficient in μm; n, polynomial order; m, meridional frequency). The defocus term (Z_2^0, #4 in single indexing scheme) was converted to equivalent diopters (D) by (2).

$$\mathrm{D} = -4\sqrt{3}\cdot\frac{\mathrm{RMS}(Z_2^0)}{r^2} \tag{2}$$

(with r, pupil radius in mm (Thibos, Hong, et al., 2002)). Due to the fact that accommodative state was uncontrolled in our setup, the true refractive state of the birds was not measured. Instead, the here presented defocus is the defocus relative to the plane of the aberrometer. Consistently, the defocus term was cancelled for any further data analyses throughout this study, unless it is stated otherwise. Astigmatism, expressed in terms of equivalent diopters of the crossed cylinder (C), was calculated from Zernike terms Z_2^2 and Z_2^{-2} by (3).

$$C = \sqrt{J_0^2 + J_{45}^2} \quad \text{with } J_0 = -2\sqrt{6}\cdot\frac{RMS(Z_2^2)}{r^2} \quad \text{and} \quad J_{45} = -2\sqrt{6}\cdot\frac{RMS(Z_2^{-2})}{r^2} \tag{3}$$

These transformations are derived from (Thibos, Hong, et al., 2002). Because measured values of pupil size were between 6.3 and 7 mm, we chose to perform our measurements with a 6-mm aperture, concentrically placed at the actual pupil. For further data analysis calculating the point spread function (PSF), the modulation transfer function (MTF), and calculating convoluted images, the best centred shots in each eye were chosen and

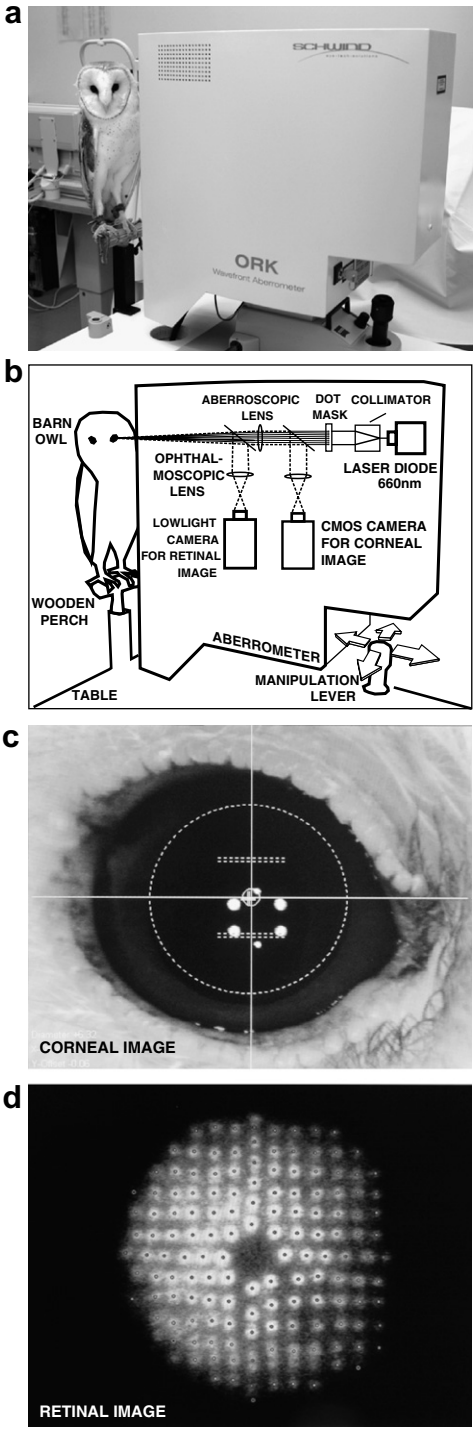

Fig. 1. (a) Owl PT in front of the aberrometer. During measurements owls were gently restrained manually by one of the experimenters to provide accurate positioning and centring of the eye in front of the aberrometer. (b) Schematic sketch of the setup and the Tscherning-system (Schwind ORK Wavefront Aberrometer). The whole system was mounted on a moving stage which was easily adjustable along all three axes in space via a manipulation lever. (c) Corneal image with superimposed aiding lines as seen online during measurements. The bright spots are first Purkinje reflexes of six IR-diodes that were circularly arranged around the aperture of the aberrometer. The dotted circular outline marks the pupil (in this image 6.32 mm diameter). (d) Typical retinal image from which the wavefront was calculated. The small dark markers within the bright illumination spots denote calculated centres of gravity for each spot.

averaged (6–10 for each eye) for all subjects separately. Convolution of a computationally designed image (vector graphic of an eye chart) was computed as follows: The original image was transformed to a greyscale bitmap and scaled in size to match the angular size of the PSF diameter calculated from the wavefront data of the according eye. The PSF was then taken as the kernel for a point-wise multiplication with the pixel neighbourhood in the original image. The calculation was performed via a two dimensional convolution in the spatial frequency domain with the Matlab function *conv2*. Convoluted images were then re-scaled, cropped to original size, and adjusted in intensity by normalization to display a saturated image.

3. Results

3.1. Raw data: Retinal illumination spot image, wavefront and single Zernike terms

During measurements pupil diameter of all eyes varied between 6.3 and 7.1 mm, which could differ for both eyes because barn owls can control pupil size in both eyes independently (Schaeffel & Wagner, 1992). Given this pupil size, the 6 mm measurement aperture could always be used, and thus, around 150 illumination spots in each retinal image were used for the calculation of the underlying wavefront. Typical image quality at the retina and arrangement of the illumination spots can be seen in Fig. 1d. Compared to studies performed with Hartmann-Shack aberrometry in humans (Liang & Williams, 1997), monkeys (Ramamirtham et al., 2006), chicken (de la Cera, Rodriguez, & Marcos, 2006), cats (Huxlin et al., 2004) and mice (de la Cera, Rodriguez, Llorente, et al., 2006), illumination spot quality observed in our study was slightly degraded with respect to visual spot edge determination, but of comparable quality regarding spot size and numbers.

Wavefront images for third and higher order aberrations over the 6 mm pupil were extremely flat, with low amounts of higher order aberrations, and revealed a mirror-symmetry between left and right eye only in subject OL and PT (see Fig. 2, first column). Single Zernike terms, shown in the second column of Fig. 2, are ordered following the OSA conventions (Thibos et al., 2000). Fig. 2 also shows higher order terms in a magnified inset. Zernike term #4 (defocus) was the largest in all eyes. The mean absolute defocus term across all subjects was 0.35 μm (STD: 0.11 μm), while the mean of absolute higher order terms was 0.012 μm (STD: 0.017 μm) across all subjects. Expressed in this way, the defocus term accounted for 96.6 % of all aberrations (second- to sixth-order) across all subjects. Aberrations up to the sixth-order were present but contributed only in a minor fashion to total wavefront error.

3.2. Second-order aberrations

With reference to the plane of the aberrometer, the eyes of three owls displayed negative defocus. Mean spherical equivalent for defocus (Zernike term #4) was between −0.12 and −0.40 D for subjects BD, OL and PT (see Fig. 3). Interocular variability was similar to inter-individual

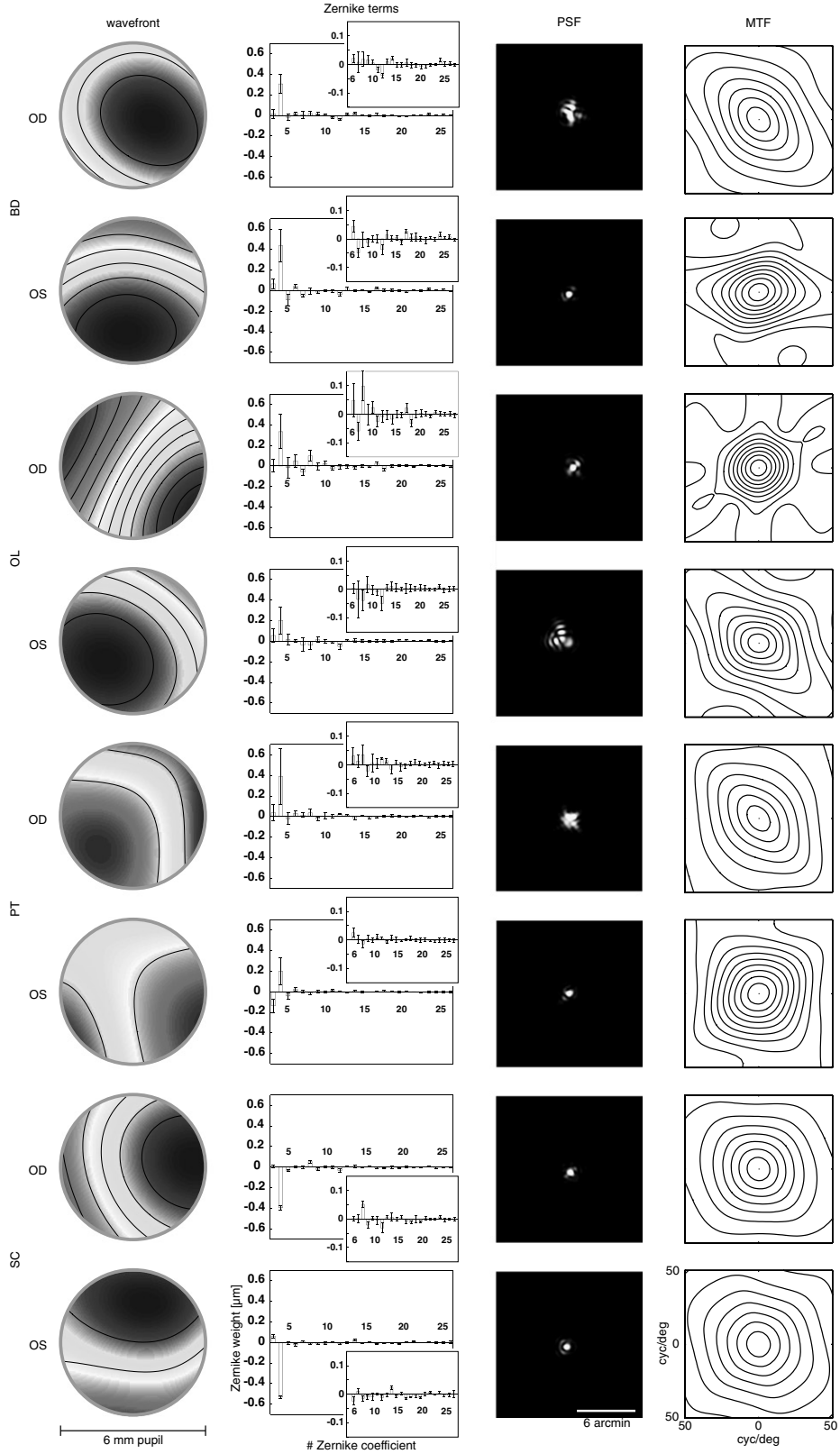

Fig. 2. First column are wavefront maps calculated from Zernike third order aberrations and higher order aberrations. Note that lines are only 0.05 μm apart. Zernike coefficients, shown in the second column, are ordered in single indexing scheme following OSA convention, error bars are standard deviations. Zernike coefficients 0 to 2 are not shown. Small inset in the upper right corner are third to sixth Zernike orders. Point-spread functions (PSF) with cancelled defocus term (Z_2^0 set to zero) are shown in the third column. They were normalized in intensity to display saturated images. In modulation transfer function (MTF) plots the lines are in steps of 0.1 modulation transfer units. Defocus was cancelled. All data are calculated for 6 mm pupils and a 660 nm illumination.

variability. Mean standard deviation in these subjects was 0.12 D. On the other hand, subject SC showed similar defocus magnitude, but with opposite sign (OS: +0.40 D, OD: +0.30 D). Mean standard deviation was comparably small (0.013 D). Astigmatism was calculated for all eyes from Zernike terms #3 and #5 according to Eq. (3), and combined to a spherical equivalent of the crossed cylinder between 0.014 and 0.065 D (mean: 0.033 D, STD: 0.020 D). Across all subjects, no clear astigmatism axis was observable.

3.3. Higher order aberrations

Generally, higher order aberrations (HOA) measured in this study were very low. To compare the impact of astigmatism and higher order aberrations on total wavefront error, the root mean square wavefront error (RMS) for the two second order terms (crossed cylinder astigmatism) are plotted together with the RMS of third- to sixth-order terms (referred to as the HOA) in Fig. 4. Second-order RMS was between 0.018 μm (OD in OL) and 0.140 μm (OS in SC). Mean second-order RMS was 0.061 μm, with a standard deviation of 0.044 μm. The HOA RMS was between 0.04 μm (OD in PT) and 0.15 μm (OS in BD), with a mean of 0.088 μm and a standard deviation of 0.033 μm. Zernike term #12 (spherical aberration term) was positive in 6 eyes and negative in the others, with a mean of 0.025 μm (STD: 0.016 μm).

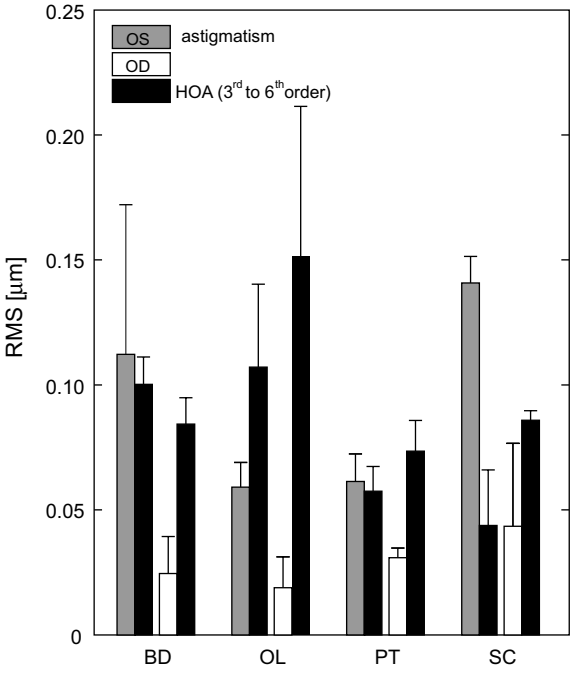

Fig. 4. Lower and higher order aberrations. The second-order RMS (without defocus) is plotted together with third- to sixth-order RMS (HOA) for each eye in all animals. Error bars denote standard deviations across measurements.

3.4. PSFs, retinal image quality and MTFs

We calculated the point-spread function (PSF) for each eye separately from the averaged Zernike terms of the best centred shots available (6–10 each). PSF plots for each subject are shown in column 3 of Fig. 2. The PSFs were calculated with cancelled defocus (Zernike term #4 computationally set to 0 μm). The PSFs after focus correction were extremely centred and resembled the diffraction limited PSF in four eyes, while in the other four eyes slight decentring and typical astigmatism effects were observed (compare OS in subject OL). In Fig. 5 a more direct comparison between owl (OS in subject BD), human, and the diffraction limited PSF is shown. Again, PSF plots are the 'best focus' PSFs. The influence of astigmatism and higher order aberrations on retinal image quality can also be observed in a set of computationally derived images. Fig. 5 (bottom right) shows a vector graphic resembling a Snellen acuity chart often used in human visual acuity tests. The gaps between the smallest letters reading the words 'BARN OWL' subtend 1 arcmin, making them the 20/20 acuity benchmark. The other charts in this figure are derived from a two-dimensional convolution of the original image with the PSF kernel presented at the top. To better identify differences between the two versions (owl vs. human), a cut-out magnification is shown as well. As a conclusion based solely on retinal image quality, both human and owl should be able to identify the smallest letters presented in this chart.

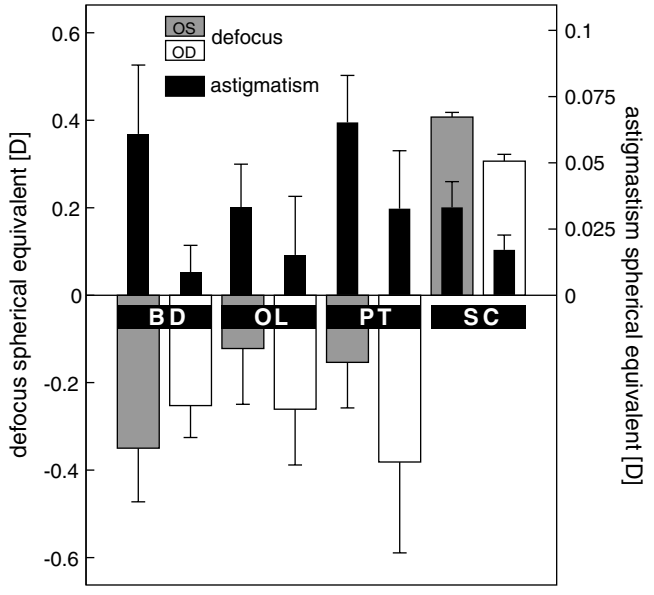

Fig. 3. Defocus and astigmatism. Spherical error derived from Zernike term Z_2^0 (defocus) and terms Z_2^2 and Z_2^{-2} (astigmatism, crossed cylinder) expressed in units of spherical equivalent in all subjects and eyes. Error bars denote standard deviations across measurements. Note the two different ordinates for defocus and astigmatism.

The complete two-dimensional modulation transfer functions (MTFs) for the 6 mm pupil of all eyes are plotted in the rightmost column of Fig. 2 (second- to sixth-orders, defocus term cancelled). Two radial cross-sections (x and y

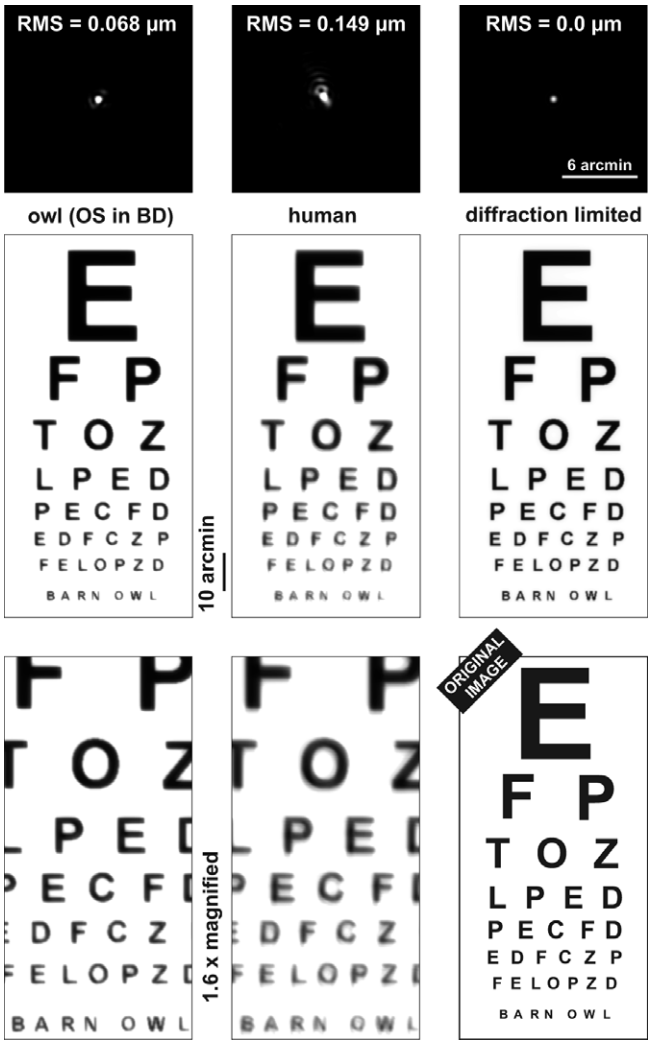

Fig. 5. Comparing PSFs and retinal image quality. Top row: exemplary PSF in owl BD (OS), PSF of a human subject, and for the diffraction limited pupil. PSFs were calculated for the best focus condition (Zernike term #4 set to zero), and for a 6 mm pupil. The total RMS (second- to sixth-orders without defocus) is shown. Middle row: A theoretical representation of retinal image quality derived from the convolution of the original image (bottom left) for the best focus condition in the owl (left), the human eye (middle), and the diffraction limited eye (right) is shown. The 'BARN OWL'-line corresponds to a 20/20 vision eye chart character size. In the bottom row (left and middle) a cut-out magnification (1.6×) is shown.

direction of Fig. 2) of the MTF for all eyes are averaged and plotted in Fig. 6 (thin dashed lines). The diffraction limited 6 mm pupil is plotted for reference as well. For comparison, the mean MTF of all owl eyes are plotted together with the mean MTF of two human subjects which participated in this study as well (pupil size was scaled to 6 mm with a re-converted Taylor polynomial). Again, only the defocus-corrected condition is shown. Note that the two human subjects had 20/20 vision. Both human and owl mean modulation transfers (MTs) are almost identical across all spatial frequencies. The owl MT exceeds human MT slightly below 20 cyc/deg and falls short of human MT above 30 cyc/deg.

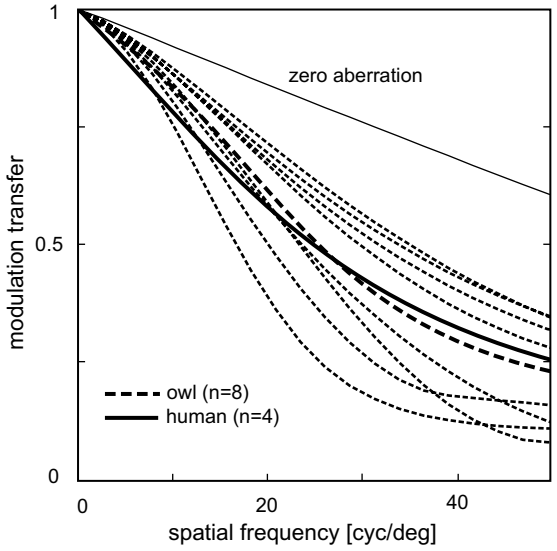

Fig. 6. MTFs in owls and humans. The cross-sectional averaged MTFs of all eyes measured in this study are presented for second- to sixth-order Zernike orders (thin dashed lines). The averaged MTF of all owl eyes is given (thick dashed line) together with the mean of four human MTFs (thick solid line). All MTFs are calculated for a 6 mm pupil with cancelled defocus. The diffraction limited eye is shown for reference. Note that the two human subjects had 20/20 vision.

4. Discussion

4.1. Methods

To our best knowledge, the here presented data is the first animal eye wavefront-error study carried out with a Tscherning-type wavefront sensor (TTWS). In recent publications of wavefront measurements in different animals the Hartmann–Shack sensor (HSS) is used most frequently (de la Cera, Rodriguez, Llorente et al., 2006; de la Cera, Rodriguez, & Marcos, 2006; Huxlin et al., 2004; Ramamirtham et al., 2006, 2003; Thibos, Cheng, et al., 2002). Nonetheless, results from TTWSs are of comparable acuity and reproducibility (Mrochen et al., 2000), especially when larger pupils are measured, because the typical lower spatial resolution in TTWS becomes negligible with larger pupil area. Throughout the literature several examples for the use of TTWS can be found (Jahnke, Wirbelauer, & Pham, 2006; Kaemmerer, Mrochen, Mierdel, Krinke, & Seiler, 2000; Krueger, Mrochen, Kaemmerer, & Seiler, 2001; Mierdel, Kaemmerer, Mrochen, Krinke, & Seiler, 2001; Mierdel, Krinke, Wiegand, Kaemmerer, & Seiler, 1997; Mrochen, Jankov, Bueeler, & Seiler, 2003; Mrochen et al., 2000; Prieto, Vargas-Martin, Goelz, & Artal, 2000). Generally, benefits from the use of TTWSs are that the ingoing light path is used for measurement and that the illumination light source lies in the visible part of the spectrum. HSSs are more frequently used in state-of-the-art wavefront measurement applications, because they are less sensitive to scattering, and usually perform at higher resolution.

One of the key requirements in wavefront analysis is the alignment of the subjects visual axis with the optical axis of the measurement system (Thibos, Applegate, et al., 2002). We achieved this with control of head position and orientation while constantly monitoring pupil size and shape. A misalignment in x–y position would have resulted in a non-centred pupil, a misalignment about any of the two torsional eye axes in yaw and pitch direction would have resulted in an ellipsoid pupil shape. This procedure of correct eye positioning is possible in the barn owl, because this animal has an extremely limited potential in moving its eyes relative to its head (DuLac & Knudsen, 1990; Knudsen & Knudsen, 1985; Knudsen & Konishi, 1979; Masino & Knudsen, 1993; Steinbach & Money, 1973).

4.2. Implications of the results

Although a small fixation cross was shown to the eye under test during the experiments, it remains unclear, whether the animals accommodated correctly with reference to the plane of the aberrometer. Due to the fact that accommodative state was not measured independently, and the barn owl generally displays a relatively high accommodative range of about 6–12 D (Howland, Howland, Schmid, & Pettigrew, 1991; Schaeffel & Wagner, 1992), the here measured relative defocus was omitted from further analyses. Without drawing conclusions about normal defocus from our data, results from an earlier developmental study in barn owls showed, that refractive errors larger than 1 D disappeared during the first two weeks of juvenile development in this animal (Schaeffel & Wagner, 1996).

Despite the uncertainty of the true amount and sign of defocus in barn owl eyes, all animals show little amounts of astigmatism and very little higher order aberrations. Typical values of HOA in humans are about 3.3 times larger than HOA reported here (Howland, 2002; Porter, Guirao, Cox, & Williams, 2001). Also, HOA in eyes of another nocturnal species, the cat, are about 3.7 times larger than those of the owl (Huxlin et al., 2004). While HOA are lower in the barn owl compared to those in human eyes in an absolute sense, this difference might become even more prominent when put into relation with absolute eye size. Axial length of barn owl eyes is about 3/4 of that of human eyes (17.5 vs. 24.5 mm, (Hughes, 1977; Schaeffel & Wagner, 1996)), and following an observation by Howland, with the same set of optics and pupil size, the wave aberrations in the smaller eye should be larger than in the bigger one (Howland, 2005).

We also showed typical PSFs of the owl eye and compared it to that derived from one human subject. Convoluted images revealed that theoretical retinal image quality is comparable in man and owl (compare also (Artal, 1990)). Mean modulation transfer of all tested owl eyes almost exactly matched modulation transfer in the two human subjects we included in this study. Taken together, the data presented here show that averaged retinal image quality in the eyes of barn owls is excellent.

Nevertheless, based on retinal ganglion cell counts, barn owls show only poor grating acuity of about 7.8 cyc/deg (Oehme, 1961; Wathey & Pettigrew, 1989). This finding is supported by a pattern electro-retinogram study which calculates grating acuity to be 6.98 cyc/deg in the barn owl (Ghim & Hodos, 2006). The question arising from these findings is why the optics of the owl's eye would have evolved in a fashion allowing the formation of a retinal image with a quality that is far beyond a visual acuity given by the neural components creating vision in this bird. A similar question has been discussed in a recent study measuring the optical quality in cat eyes (Huxlin, Yoon, Nagy, Porter, & Williams, 2004). The authors propose that given the nocturnal lifestyle of the cat combined with an almost three times larger pupil area in cats compared to humans at the same light levels, cats should experience significantly more optical interference than humans at the same light level. The authors conclude that the cat's optics are relatively good because otherwise additional aberrations would degrade vision to levels of unsustainability (Huxlin, Yoon, Nagy, Porter, & Williams, 2004). Given the relatively low high-frequency visual acuity in the barn owl (below 10 cyc/deg), this argument might not stand up to a quantitative analysis. On the other hand, being equipped with excellent optics that raise the MTF over all spatial frequencies, the owl might take advantage from an elevated contrast sensitivity for low spatial frequencies close to its neural sample pattern (compare Fig. 6). Thus, while flying in the dark, owls might better manoeuvre through and avoid hitting low spatial frequency objects like e.g. limbs of a tree, and better visually identify items of prey. As an example, a mouse (6 cm) viewed from typical striking distance (5 m) would subtend about 0.7 cyc/deg, which matches the owl's contrast sensitivity function peak quite well (Ghim & Hodos, 2006).

Acknowledgments

The authors thank Schwind Eye Tech Solutions for their technical support on raw data extraction. We also thank Patrick Maeda for generous help with preparing some of the figures. The authors especially thank two anonymous referees for helpful comments on an earlier version of the manuscript.

References

Artal, P. (1990). Calculations of two-dimensional foveal retinal images in real eyes. *Journal of the Optical Society of America A, 8*, 1374–1381.

Banton, T., & Levi, D. M. (1991). Binocular summation in vernier acuity. *Journal of the Optical Society of America. A, Optics Image Science and Vision, 4*, 673–680.

Coletta, N. J., Troilo, D., Moskowitz, A., Nickla, D. L., & Marcos, S. (2003). Wavefront aberrations of the marmoset eye. *Investigative Ophthalmology & Visual Science*, U324.

de la Cera, E. G., Rodriguez, G., Llorente, L., Schaeffel, F., & Marcos, S. (2006). Optical aberrations in the mouse eye. *Vision Research, 16*, 2546–2553.

de la Cera, E. G., Rodriguez, G., & Marcos, S. (2006). Longitudinal changes of optical aberrations in normal and form-deprived myopic chick eyes. *Vision Research, 4*, 579–589.

DuLac, S., & Knudsen, E. I. (1990). Neural maps of head movement vector and speed in the optic tectum of the barn owl. *Journal of Neurophysiology, 1*, 131–146.

Ghim, M. M., & Hodos, W. (2006). Spatial contrast sensitivity of birds. *Journal of Comparative Physiology. A, Neuroethology Sensory Neural, and Behavioral Physiology, 5*, 523–534.

Harmening, W. M., Göbbels, K., & Wagner, H. (2007). Vernier acuity in barn owls. *Vision Research, 7*, 1020–1026.

Howland, H. C. (2005). Allometry and scaling of wave aberration of eyes. *Vision Research, 9*, 1091–1093.

Howland, H. C. (2002). High order wave aberration of eyes. *Ophthalmic & Physiological Optics, 5*, 434–439.

Howland, H. C., Howland, M. J., Schmid, K., & Pettigrew, J. D. (1991). Restricted range of ocular accommodation in barn owls (Aves, Tytonidae). *Journal of Comparative Physiology. A, Sensory Neural and Behavioral Physiology, 3*, 299–303.

Howland, H. C., Merola, S., & Basarab, J. R. (2004). The allometry and scaling of the size of vertebrate eyes. *Vision Research, 17*, 2043–2065.

Hughes, A. (1977). The topography of vision in mammals of contrasting life style: Comparative optics and retinal organisation, VII/5, 613–656.

Huxlin, K. R., Yoon, G., Nagy, L., Porter, J., & Williams, D. (2004). Monochromatic ocular wavefront aberrations in the awake-behaving cat. *Vision Research, 18*, 2159–2169.

Jahnke, M., Wirbelauer, C., & Pham, D. T. (2006). Influence of age on optical aberrations of the human eye. *Ophthalmologe, 7*, 596–604.

Kaemmerer, M., Mrochen, M., Mierdel, P., Krinke, H. E., & Seiler, T. (2000). Clinical experience with the Tscherning aberrometer. *Journal of Refractive Surgery, 5*, S584–S587.

Knudsen, E. I., & Knudsen, P. F. (1985). Vision guides the adjustment of auditory localization in young barn owls. *Science, 4725*, 545–548.

Knudsen, E. I., & Konishi, M. (1979). Mechanisms of sound localization in the barn owl (Tyto-Alba). *Journal of Comparative Physiology, 1*, 13–21.

Krueger, R. R., Mrochen, M., Kaemmerer, M., & Seiler, T. (2001). Understanding refraction and accommodation through 'retinal imaging' aberrometry—A case report. *Ophthalmology, 4*, 674–678.

Liang, J. Z., & Williams, D. R. (1997). Aberrations and retinal image quality of the normal human eye. *Journal of the Optical Society of America. A, Optics Image Science and Vision, 11*, 2873–2883.

Malania, M., Herzog, M. H., & Westheimer, G. (2007). Grouping of contextual elements that affect Vernier thresholds. *Journal of Vision, 2*, 1–7.

Marcos, S. (2006). Aberrometry: basic science and clinical applications. *Bulletin de la Societe Belge d Ophthalmologie (Brussels), 302*, 197–213.

Martin, G. R. (1984). The visual-fields of the tawny owl, Strix-Aluco l. *Vision Research, 12*, 1739–1741, 1743–1751.

Martin, G. R. (1982). An owls eye—Schematic Optics and Visual Performance in Strix-Aluco l. *Journal of Comparative Physiology, 3*, 341–349.

Martin, G. R., & Katzir, G. (1999). Visual fields in short-toed eagles, *Circaetus gallicus* (Accipitridae), and the function of binocularity in birds. *Brain Behavior and Evolution, 2*, 55–66.

Masino, T., & Knudsen, E. I. (1993). Orienting head movements resulting from electrical microstimulation of the brain-stem tegmentum in the barn owl. *Journal of Neuroscience, 1*, 351–370.

Mierdel, P., Kaemmerer, M., Mrochen, M., Krinke, H. E., & Seiler, T. (2001). Ocular optical aberrometer for clinical use. *Journal of Biomedical Optics, 2*, 200–204.

Mierdel, P., Krinke, H. E., Wiegand, W., Kaemmerer, M., & Seiler, T. (1997). A measuring device for the assessment of monochromatic aberrations in human eyes. *Ophthalmologe, 6*, 441–445.

Mrochen, M., Jankov, M., Bueeler, M., & Seiler, T. (2003). Correlation between corneal and total wavefront aberrations in myopic eyes. *Journal of Refractive Surgery, 2*, 104–112.

Mrochen, M., Kaemmerer, M., Mierdel, P., Krinke, H. E., & Seiler, T. (2000). Principles of Tscherning aberrometry. *Journal of Refractive Surgery, 5*, S570–S571.

Nieder, A., & Wagner, H. (2001). Encoding of both vertical and horizontal disparity in random-dot stereograms by Wulst neurons of awake barn owls. *Visual Neuroscience, 4*, 541–547.

Nieder, A., & Wagner, H. (1999). Perception and neuronal coding of subjective contours in the owl. *Nature Neuroscience, 7*, 660–663.

Oehme, H. (1961). Vergleichend-histologische Untersuchung an der Retina von Eulen. *Zoologische Jahrbücher für Anatomie, 79*, 439–478.

Pettigrew, J. D., & Konishi, M. (1976). Neurons selective for orientation and binocular disparity in the visual Wulst of the barn owl (*Tyto alba*). *Science, 4254*, 675–678.

Porter, J., Guirao, A., Cox, I. G., & Williams, D. R. (2001). Monochromatic aberrations of the human eye in a large population. *Journal of the Optical Society of America. A, Optics Image Science and Vision, 8*, 1793–1803.

Prieto, P. M., Vargas-Martin, F., Goelz, S., & Artal, P. (2000). Analysis of the performance of the Hartmann–Shack sensor in the human eye. *Journal of the Optical Society of America. A, Optics Image Science and Vision, 8*, 1388–1398.

Ramamirtham, R., Kee, C. S., Hung, L. F., Qiao-Grider, Y., Roorda, A., & Smith, E. L. III, (2006). Monochromatic ocular wave aberrations in young monkeys. *Vision Research, 21*, 3616–3633.

Ramamirtham, R., Kee, C. S., Qiao-Grider, Y., Hung, L. F., Ward, M., & Smith, E. L. (2005). Corneal and internal wave aberrations in normal rhesus monkeys (*Macaca mulatta*). *Investigative Ophthalmology & Visual Science*.

Ramamirtham, R., Norton, T. T., Siegwart, J. T., & Roorda, A. (2003). Wave aberrations of tree shrew eyes. *Investigative Ophthalmology & Visual Science*, U324.

Schaeffel, F., & Wagner, H. (1992). Barn owls have symmetrical accommodation in both eyes, but independent pupillary responses to light. *Vision Research, 6*, 1149–1155.

Schaeffel, F., & Wagner, H. (1996). Emmetropization and optical development of the eye of the barn owl (*Tyto alba*). *Journal of Comparative Physiology. A, Sensory Neural and Behavioral Physiology, 4*, 491–498.

Steinbach, M. J., & Money, K. E. (1973). Eye-movements of the owl. *Vision Research, 4*, 889–891.

Thibos, L. N., Applegate, R. A., & Marcos, S. (2003). Aberrometry: The past, present, and future of optometry. *Optometry and Visual Science, 1*, 1–2.

Thibos, L. N., Applegate, R. A., Schwiegerling, J. T., & Webb, R. (2002). Standards for reporting the optical aberrations of eyes. *Journal of Refractive Surgery, 5*, S652–S660.

Thibos, L. N., Applegate, R. A., Schwiegerling, J. T., & Webb, R. (2000). Report from the VSIA taskforce on standards for reporting optical aberrations of the eye. *Journal of Refractive Surgery, 5*, S654–S655.

Thibos, L. N., Cheng, X., Phillips, J. R., & Collins, A. (2002). Optical aberrations of chick eyes. *Investigative Ophthalmology & Visual Science, 43*, *[E-Abstract 180]*.

Thibos, L. N., Hong, X., Bradley, A., & Cheng, X. (2002). Statistical variation of aberration structure and image quality in a normal population of healthy eyes. *Journal of the Optical Society of America. A, Optics Image Science and Vision, 12*, 2329–2348.

van der Willigen, R. F., Frost, B. J., & Wagner, H. (1998). Stereoscopic depth perception in the owl. *Neuroreport, 6*, 1233–1237.

van der Willigen, R. F., Frost, B. J., & Wagner, H. (2003). How owls structure visual information. *Animal Cognition, 1*, 39–55.

Wagner, H., & Frost, B. (1994). Binocular responses of neurons in the barn owls visual wulst. *Journal of Comparative Physiology, A. Sensory Neural and Behavioral Physiology, 6*, 661–670.

Wagner, H., & Frost, B. (1993). Disparity-sensitive cells in the owl have a characteristic disparity. *Nature, 6440*, 796–798.

Wagner, H., & Luksch, H. (1998). Effect of ecological pressures on brains: Examples from avian neuroethology and general meanings. *Zeitschrift fur Naturforschung C—A Journal of Biosciences, 7–8*, 560–581.

Wathey, J. C., & Pettigrew, J. D. (1989). Quantitative analysis of the retinal ganglion cell layer and optic nerve of the barn owl *Tyto alba*. *Brain Behavoir and Evolution, 5*, 279–292.